Polymers for Advanced Technologies

WILEY

polymers advanced technologies

RESEARCH ARTICLE OPEN ACCESS

Advancing Mechanical Properties of Polypropylene Matrix Composites: Analysis of Diverse Reinforcing Fillers

Ali Sadooghi[1] | Seyed Jalal Hashemi[1] | Vahid Zal[2] | Farzad Rahmani[3] | Kaveh Rahmani[4] | Mahdi Bodaghi[4]

[1]Department of Mechanical Engineering, National University of Skills, Tehran, Iran | [2]Department of Mechanical Engineering, Qom University of Technology, Qom, Iran | [3]Department of Mechanical Engineering, Kar Higher Education Institute, Qazvin, Iran | [4]Department of Engineering, School of Science and Technology, Nottingham Trent University, Nottingham, UK

Correspondence: Ali Sadooghi (a.sadooghi@sru.ac.ir) | Mahdi Bodaghi (mahdi.bodaghi@ntu.ac.uk)

Received: 8 October 2024 | **Revised:** 20 December 2024 | **Accepted:** 24 December 2024

Funding: The authors received no specific funding for this work.

Keywords: composite additives | mechanical properties | polymer composites | reinforced polypropylene

ABSTRACT

Currently, much research is being conducted on increasing the strength of thermoplastic polymers using various additives. Polypropylene (PP) is widely used in the automotive industry and electrical equipment. In this paper, using various reinforcing particles/fibers, including calcium carbonate, $CaCO_3$, (at 20%, 25%, and 30% weight percentages), 20% talc, and 20% barite particles, as well as 30% glass fibers (GFs) (with varying L/D ratios, 200, 250, and 300) were integrated. First, PP and additives were mixed homogeneously by an extrusion process, and then test samples were made by high-pressure injection of the extruded product into the mold. Various tests, including tensile, impact, and melt flow index (MFI) tests, were conducted to investigate the effect of additives on the properties of composites produced by plastic injection molding. SEM analysis was used to examine the fracture cross-section of the samples and the distribution of additives. Results revealed significant outcomes across multiple tests: the addition of reinforcing particles led to a reduction in yield strain while creating notable variations in yield strength. Charpy impact tests demonstrated varied energy absorption, with the highest observed in the 30% GF sample (with L/D ratio of 350). Furthermore, the incorporation of reinforcing particles and fibers increased the heat deflection temperature, with the 30% GF sample exhibiting the highest value. Additionally, reinforcements effectively mitigated shrinkage, with significant reductions noted in samples containing talc and GF. The PP sample displayed a shrinkage rate of 19.1%. This figure significantly decreased to 1.42% and 0.26% for the samples reinforced by talc and GF [L/D = 350]. Furthermore, the introduction of GFs resulted in a decreased MFI, while other particles exhibited minimal impact.

1 | Introduction

Composite materials are constructed through the physical amalgamation of two or more components at a macroscopic level. Within this blend, the interface between these components persists, preserving the distinct identity of each. Typically, composites comprise two primary phases: a continuous matrix and a dispersed reinforcement [1]. The continuous phase serves as a binder, securely housing the reinforcing particles akin to glue. When subjected to force, this matrix undergoes deformation, effectively transferring stress to the dispersed reinforcement. The additional components are introduced to fortify the composites, imparting unique characteristics to the resulting material [2]. Polymer matrix composites, renowned for their versatility and adaptability, are reclaiming their position as essential elements in the realm of construction materials. Among these, polypropylene (PP) stands out with its versatile applications but is hindered by its limited impact strength, particularly in lower temperatures [3]. To address this limitation and meet the technical demands of engineering applications, PP is commonly

blended with various reinforcements to enhance mechanical properties, processing ease, and cost-efficiency [4].

Up until now, significant research has been conducted to ascertain the effects of adding reinforcing materials to PP matrix composites on the material properties: Baek et al. [5] investigated how β-SiC nanoparticle clustering affects electrical conductivity in PP composites. Their innovative approach, combining calculations and homogenization, unveiled a clear relationship between nanoparticle dispersion and conductivity. Notably, agglomerated β-SiC particles significantly boosted conductivity compared to dispersed ones, attributed to their unique work function. Zal et al. [6] present a new method to analyze the short fibers' alignment inside resin layers using in situ measuring of light transmission. An important finding is that the ratio of fiber length and resin thickness showcases a limit to the alignment degree. Also, they did an analytical model to predict average fiber angles based on the sample configuration. Zal et al. [7] investigated the effects of processing parameters, including temperature, time, and pressure on the properties of amorphous polyvinyl chloride (PVC)/fiberglass thermoplastic composite laminates. The film stacking and hot pressing procedure was used to produce the composite laminates. The results showed that the processing temperature has the maximum effect on the product strength, and an increase of the temperature up to 230°C increases the flexural strength. On the other hand, higher temperature results in matrix degradation and strength reduction. Begum et al. [8] investigated natural and synthetic fiber-reinforced polymer matrix composites. Their study addressed environmental concerns linked with synthetic fibers and the rising interest in eco-friendly alternatives such as kenaf and jute. They observed that natural fiber-reinforced PMCs demonstrated improved mechanical properties, suggesting their applicability across various fields. Małek et al. [9] investigated the incorporation of glass waste into cement composites to enhance sustainability. They explored the use of glass powder and aggregate as substitutes for traditional components, aiming to reduce energy consumption and CO_2 emissions in concrete production. Results showed significant enhancements in flexural and splitting strength with increasing fiber content, indicating the potential of recycled macro-polymer fibers in enhancing mechanical properties. Ari et al. [10] conducted a comparative study on the mechanical properties of PP composites reinforced with chopped glass, carbon, and aramid fibers. Tensile, three-point bending, and drop weight tests were conducted, revealing a significant enhancement in mechanical properties with fiber reinforcement, albeit with diminishing returns as fiber content increased. Statistical analyses including ANOVA and *F*-test were employed to assess the impact of fiber type and content on test results. Guo et al. [11] investigated the impact of TiO_2 nanoparticle treatment on bamboo fibers (BFs) reinforced PP composites to enhance interfacial bonding. The study evaluated static and dynamic mechanical properties, thermal stability, water resistance, and the morphology of the fabricated composites. Results indicated improvements across these properties, particularly with 0.4 wt% TiO_2 nanoparticle additions, attributed to enhanced interfacial bonding and increased crystallinity. Goud et al. [12] studied the impact of different initial states of PP matrix states (fiber, powder, film) on the flexural strength in carbon-PP composites. Their investigation highlighted superior mechanical properties in unidirectional composites produced by electrostatic spray coating (UDC-P), attributed to enhanced PP powder impregnation despite its higher viscosity, marking the first comparative study of powder coating versus DREF and film stacking methods. Hariprasad et al. [13] examined natural fiber-reinforced PP composites for automotive applications. They evaluated the mechanical properties and acoustic characteristics of PP composites. Their investigation involved various natural fibers mixed with PP and assessed mechanical attributes like tensile strength, hardness, and water absorption. The study also explored acoustic properties at different thicknesses, revealing insights into suitable materials for diverse automotive applications. Song et al. [14] focused on fabricating highly thermally conductive PP/graphene composites using a novel in situ building method for improved thermal management in electronic devices. Their approach, incorporating a three-dimensional graphene framework and a unique matrix functionalization inspired by mussel adhesion, significantly enhanced through-plane thermal conductivity, demonstrating the promising potential for efficient heat dissipation in high-power electronic devices. Oladele et al. [15] explored the impact of sodium hydroxide mercerization on bagasse fiber and its effects on the mechanical and thermal properties of PP composites reinforced with BF/$CaCO_3$ hybrids. Their study focused on characterizing tensile, flexural, and thermal properties, revealing that the mercerized BF-based hybrid composites exhibited superior mechanical and thermal traits compared to other composite variations. Hernández-Jiménez et al. [16] explored white oak wood flour's impact on PP properties, focusing on particle size and content variations. The findings highlighted increased water absorption with wood particle integration and significant effects on mechanical properties, including reduced elongation and strength, and increased modulus values. Korol et al. [17] assessed the environmental impact of PP composites filled with cotton, jute, and kenaf fibers, compared to glass fiber (GF) and unmodified PP. Incorporating 30 wt% of these natural fibers reduced the carbon footprint by 3%–18% and showed varied effects on ecological footprints. While jute and kenaf fibers improved the ecological footprint, cotton fiber increased it by 52%. Kim et al. [18] studied the impact of carbon fibers and graphite flakes on heat dissipation and mechanical strength in PP composites at various mixing ratios. They found that high thermal conductivity in graphite flakes and reinforcing mechanical strength with carbon fibers were influenced significantly by the mixing ratios. Rajkumar et al. [19] analyzed flax fiber-reinforced PP composites with varied lignite fly ash (LFA) contents. The study observed structural and mechanical changes, noting enhanced thermal stability and strength with up to 10 wt. % LFA. The 5 wt. % LFA composite displayed superior properties, presenting the potential for aerospace, construction, and automobile applications. Patel et al. [20] investigated the impact of different reinforcement loads on the mechanical properties of recycled PP matrix composites. The study examined the effects of varying fiber direction in BF composites and the addition of calcium carbonate on the mechanical properties of calcium carbonate-reinforced composites. Results revealed that BFs treated with 5% NaOH exhibited superior tensile characteristics, with a tensile strength of 507 MPa and an elasticity modulus of 10.3 GPa. Brahma et al. [21] explored the dyeability enhancement of banana fibers using synthetic dyes and investigated the mechanical properties of PP

composites reinforced with these dyed fibers. The composites, prepared by sandwiching dyed fibers between PP sheets and hot pressing, showed minor bond formations between the fibers and PP matrix, as revealed by Fourier Transform Infrared Spectroscopy analysis. While the composites demonstrated only slight enhancements in tensile strength and modulus compared to those with untreated fibers, direct and basic dyes were identified as the most suitable synthetic dyes for this purpose. Meena et al. [22] investigated the effects of fly ash incorporation on the thermo-mechanical and mechanical behavior of PP matrix composites. By varying the weight percentages of fly ash particles in PP through a twin-screw extrusion and injection molding, the study evaluated mechanical and thermal response. The results showed that the compressive strength increased initially with the addition of up to 2 wt% fly ash particles, followed by a slight decline. Tensile and flexural strength exhibited a similar trend, with improvements observed up to certain percentages of fly ash addition before declining. Longtao et al. [23] used polyphenylene ether/PP/GF composites as the matrix material to obtain the dielectric plate material and the reinforcement effect was investigated. The results showed that the compound compatibilizers improve the compatibility and performance. Then, the crystallization effect of $CaTiO_3$ fillers on the composites was investigated, and the DSC analysis revealed that using a small amount of $CaTiO_3$ promoted the crystallization of PP, while using a large amount of $CaTiO_3$ inhibited the crystallization effect. Murillo et al. [24] evaluated the influence of adding borosilicate residue as a flame retardant in PP and natural fiber composites. The composites were produced by corotational twin-screw extrusion and injection molding to obtain the test specimens, and a coating process was carried out to add the water-soluble fraction to the surface of the compositions. The addition of only 2 wt% borosilicate residue content induces an increase in thermal stability of 32°C and 109°C for composites with and without natural fibers, respectively. The addition of 20 wt% borosilicate residue elevates the elastic modulus up to 27% of the composites with and without natural fibers. This approach produces composites with improved flammability, thermal stability, and mechanical properties, making them suitable for various end applications. Balaji et al. [25] produced basalt fiber-reinforced PP composites with two initial fiber lengths (3.2 and 6.4 mm) using twin-screw extrusion compounding. Yang et al. [26] used nano-sized $CaCO_3$ particles to improve the mechanical properties and impact resistance of PP. Their results showed that adding carbonate increased the toughness of PP by up to four times. The results of a paper by Palanikumar et al. [27] showed that a 10% increase in $CaCO_3$ can increase the wear resistance of PP by 70%. Zhou et al. [28] showed that adding talc to PP increases its elastic modulus but, on the other hand, reduces the yield stress. Lapcik et al. [29] investigated the effect of adding talc in nano and micro sizes on the strength and impact resistance of PP. Their results showed that adding talc increases the tensile strength of the material but increases its brittleness. Fu et al. [30] used GF addition of up to 25% to increase the strength of PP.

As previous studies have shown, adding particles or fibers to the PP matrix can improve its mechanical and physical properties. Almost all published articles have investigated the effect of only one additive on the properties of PP. In view of this, there is a need for a comprehensive study to compare different additives and produce PP matrix composites, in such a way that various properties such as mechanical strength, impact resistance, and temperature-dependent properties of the composite are investigated to determine the best additive for different applications. This article investigates the effects of incorporating dispersed reinforcements into PP matrix composites. Additives include $CaCO_3$ with varying weight percentages, talc, barite particles, and GF with different L/D ratios. Till now, no research has been done on this variety of reinforcements. The study examines mechanical and thermal properties using experimental techniques such as tensile testing, impact testing, heat deflection temperature (HDT) measurements, shrinkage analysis, and melt flow index (MFI) assessments. Results show that the addition of reinforcing particles leads to significant changes in both mechanical properties and processing characteristics of PP matrix composites. By systematically analyzing these effects, we aim to provide valuable insights for the design and optimization of PP-based composites for specific applications.

2 | Experimental Method

2.1 | Material and Samples

The composite specimens are fabricated from a PP matrix with HP 522R specifications, fortified with various reinforcing elements including, $CaCo_3$, barite, and talc particles, and GFs to enhance the structural integrity of the PP matrix. The microparticles employed in this formulation exhibit a size of less than 100 μm and boast a purity of 99%. Additionally, the reinforcing GFs are selected with varying length-to-diameter ratios (L/D = 250, 300, and 350). Table 1 provides an overview of the produced samples, encompassing their compositions and respective proportions. The selection of reinforcing fillers and their weight percentages was based on their cost-effectiveness, availability, and potential to enhance the mechanical properties of the PP matrix.

It is worth mentioning that prior to the manufacturing process, a pretreatment procedure is executed, involving the 5-min mixture of antioxidant and wax additives (i.e., at a concentration of 1% by weight) into the matrix. The inclusion of antioxidants serves to safeguard the integrity of materials and compounds against degradation during processing, thereby preserving their molecular composition. Likewise, the addition of wax serves a dual purpose: facilitating the granulation process and mitigating frictional forces between materials and equipment.

2.2 | Production Process

To fabricate the microcomposite samples, the process begins with the introduction of PP granules into a twin-screw extrusion machine. The granules undergo melting facilitated by the heaters surrounding the machine, driven by the motion of the granules within the apparatus. Subsequently, reinforcing particles or fibers, in accordance with the specified compositions and weight percentages, are added to the molten PP matrix via a dosing system and blended thoroughly. Following thorough mixing, the molten compound mixture traverses through a vacuum chamber to eliminate any moisture and air impurities, thereby enhancing the product's

TABLE 1 | The name and composition of produced samples.

Samples	Sample compositions by weight percentage	Other additives
(PP) HP 552R	99% HP 522R	1% (Wax +Antioxidine)
20% $CaCo_3$	79% HP 522R + 20% $CaCo_3$	
25% $CaCo_3$	74% HP 522R + 25% $CaCo_3$	
30% $CaCo_3$	69% HP 522R + 30% $CaCo_3$	
20% talc	79% HP 522R + 20% talc	
20% barite	79% HP 522R + 20% barite	
GF30% [L/D = 250]	69% HP 522R + 30% GF (L/D = 250)	
GF30% [L/D = 300]	69% HP 522R + 30% GF (L/D = 300)	
GF30% [L/D = 350]	69% HP 522R + 30% GF (L/D = 350)	

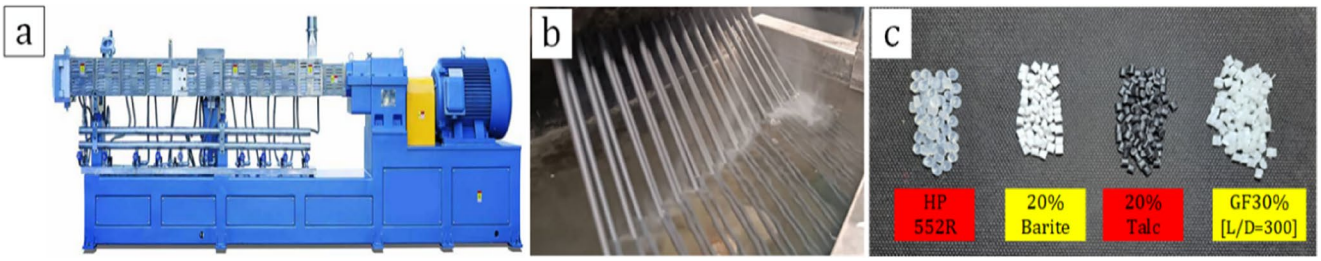

FIGURE 1 | Illustration of the extrusion process, featuring (a) the extrusion machine, (b) the dough string during extrusion, and (c) resulting granules.

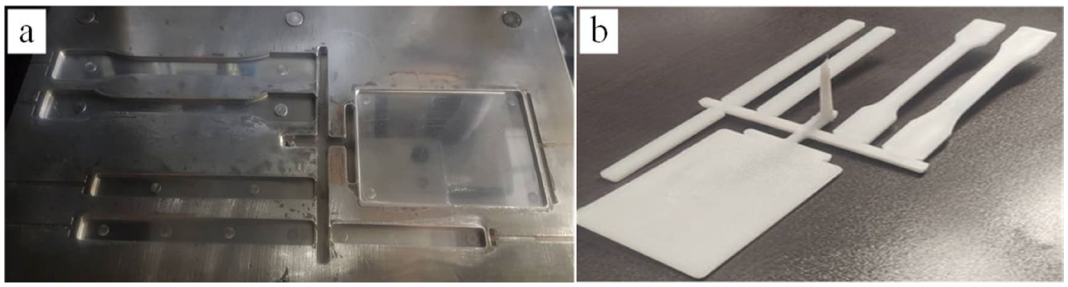

FIGURE 2 | (a) Fabricated mold and (b) the injected material within the mold.

purity. The refined molten material, endowed with kinetic and thermal energy, then traverses through the extruders, yielding granular paste, which is subsequently subjected to a water bath for cooling before being precisely cut into solid particles. Figure 1 presents a schematic depiction of the utilized extrusion machine, illustrating the dough strings and the granules of the produced compounds. The extrusion machine's heaters are calibrated to a temperature of 290°C, with a screw rotation speed set at 300 rpm and a pressure of 20 MPa during the injection process.

To facilitate the production of samples for subsequent characterization testing, PP granules are melted and injected into steel molds using a plastic injection device to fabricate standardized samples. The plastic injection process is executed at a temperature of 200°C, with an injection speed of 25 g/min and pressure of 70 MPa. Figure 2 illustrates the fabricated mold and the resulting injected samples.

2.3 | Characterization Tests

2.3.1 | Tensile Testing

The tensile test was conducted using the Testometric M350-10AT model apparatus in accordance with the ISO 527-1 standard. Tensile test samples were subjected to a strain rate of 5 mm/min until failure occurred (Figure 3).

2.3.2 | Cahrpy Impact Test

The Charpy impact test serves to evaluate the impact strength and fracture toughness of a material. This test was conducted on specimens featuring a cross-sectional area of 10 × 10 mm and a total length of 55 mm, with a V-shaped notch positioned at the center. The 45° notch boasts a 2 mm deep, and a radius

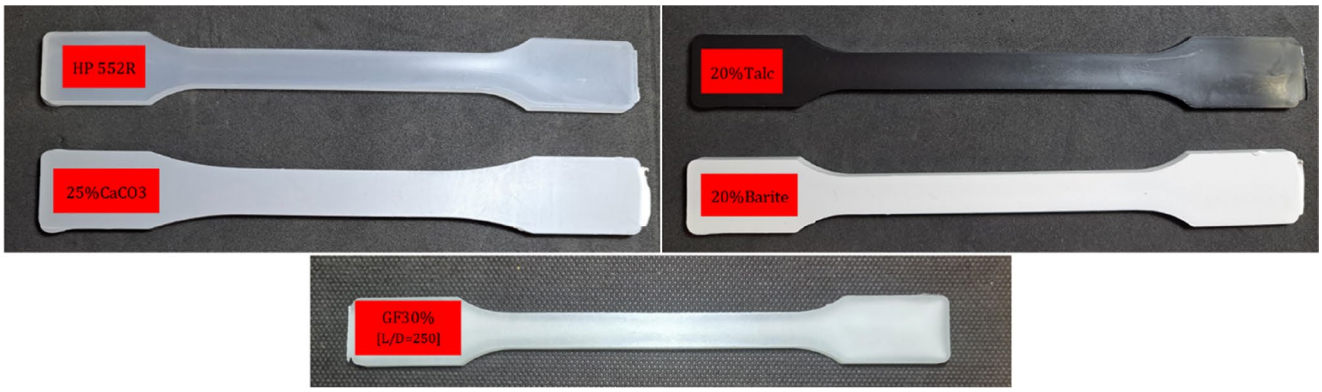

FIGURE 3 | The produced samples intended for tensile testing.

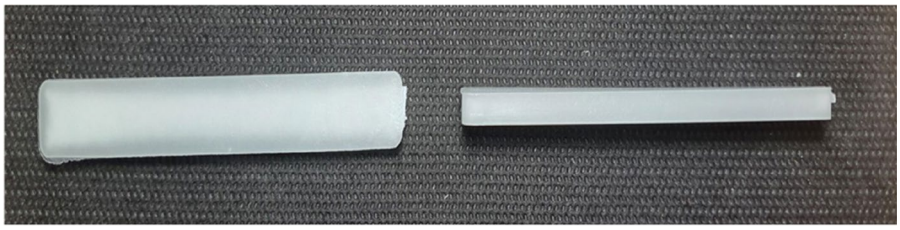

FIGURE 4 | The shrinkage test sample of GF30% [L/D = 350].

of curvature equal to 0.25 mm, adhering to the ISO 179-1 standard.

2.3.3 | HDT Test

The HDT test aims to ascertain the HDT in polymer samples under constant loading conditions. Hence, samples are positioned within a silicone oil bath, with an applied weight of 230 g, according to the ISO 75 standard. The device incrementally raises the temperature of the silicone oil at a rate of 2°C/min. The bending characteristics of the samples are measured by an inserted gauge until reaching 0.34 mm allowed deflection, at which point the temperature is deemed as the HDT of the sample.

2.3.4 | Shrinkage Test

In the shrinkage test, the contraction of a polymer sample volume during the cooling stage of fabrication is measured. This phenomenon arises due to differences in density between the solid and molten states of polymers, typically occurring during the cooling phase of polymer-injected samples, once temperature and humidity stabilization conditions are achieved. The test protocol adheres to the ASTM D955 standard. Figure 4 displays the GF30% [L/D = 350] sample for the shrinkage test, captured from two angles. The samples are kept in the laboratory environment after 24 h of injection, and then, precise measurements of both the sample and mold dimensions are conducted, and the percentage of shrinkage is calculated using Equation (1):

$$\text{Shrinkage}\,(\%) = \frac{(\text{Mold's length} - \text{sample's length})}{\text{Mold's length}} \times 100 \quad (1)$$

2.3.5 | MFI Test

The MFI test evaluates the melt flow characteristics of a thermoplastic polymer, serving as an indicator of the sample's extrudability. A high MFI can result in "flashing", while a low MFI indicates inadequate fluidity, leading to incomplete mold filling. Generally, as the MFI increases, the tensile strength, softening temperature, and toughness of the polymer decrease. The MFI test, conducted in accordance with the ASTM D1238 standard, involves extruding the melted material through an orifice by applying a weight of 2160 g onto the molten material. The weight of the extruded material over a 10-min period is recorded and then multiplied by 20 to obtain the MFI value (grams per 10 min). Figure 5 depicts a sample obtained following the MFI test.

2.3.6 | Ash Content Test

Upon exposure to high temperatures, polymer materials undergo combustion, resulting in the formation of ash residues. To determine the ash content within the materials under investigation, an ash content test is performed in accordance with the ASTM D5630 standard. Initially, the crucible is placed in an oven set at 950°C for 10 min, followed by transferring them to a desiccator to ensure thorough drying without moisture absorption or dust contamination. Subsequently, the weight of the crucible is measured. A crushed portion of a sample is then introduced into the crucible, and the weight is remeasured. The crucible, along with the sample, is subjected to heat until complete combustion occurs, and the resulting smoke dissipates. The crucible containing the residual ash, along with the sample, is then placed in the oven for 30 min before being transferred to the desiccator to reach ambient temperature. The final weight is measured, and the ash content is calculated using Equation (2):

$$\text{Ash content} = \frac{M_o}{M_1} \times 100 \quad (2)$$

where M_0 represents the remaining ash in the crucible and M_1 denotes the initial sample weight, all measured in grams. Additionally, Figure 6 depicts the furnace, the crucible, and the ash residue from the samples inside the crucible.

2.3.7 | Scanning Electron Microscope

Following the amalgamation of materials and their injection into the molds, the primary objective was to ensure proper dispersion of the reinforcing particles and fillers within the (PP) HP 552R matrix. After the tensile test, the fracture cross-section of the samples was studied by scanning electron microscope (SEM). So, the samples were prepared by sectioning with approximately a length and height of 10 mm with the thickness of the tensile test specimen. Then, gold coating was done on the surface of the samples for SEM-EDS analysis.

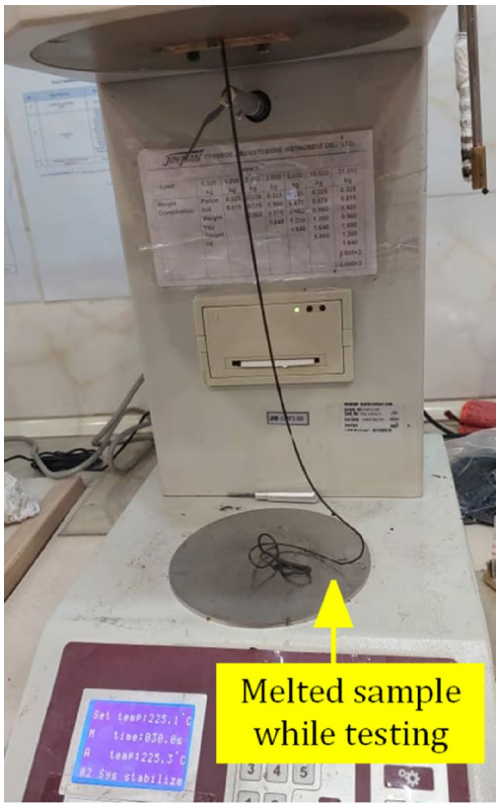

FIGURE 5 | A sample following the Melt Flow Index (MFI) test.

3 | Results and Discussion

3.1 | Microstructural Analysis

Figure 7 presents significant observations, where filler particles and reinforcing fibers are delineated by yellow circles and some random points, respectively, indicating their successful bonding to the PP matrix, as marked by red circles. Overall, the images illustrate adequate dispersion of particles/fibers throughout the matrix. Furthermore, EDS results depict the presence of C and N elements in all samples, attributable to the constituent elements of HP 552R (PP). The detection of C elements in samples containing 20%, 25%, and 30% $CaCo_3$ is attributed to the reinforcing fillers as well. The EDS analysis confirms the presence of S and Ba elements in barite-reinforcing particles. Additionally, the presence of Si and Ca elements in samples reinforced with GFs and $CaCo_3$ is evident. Finally, the gold coating material is detected in all samples at beam energies of 2 and 10 keV.

3.2 | Tensile Test

The tensile test was performed on both pure PP (i.e., without any added reinforcing particles or fibers) and reinforced PP samples to evaluate their tensile behavior, as detailed in Table 2. Given the significance of yield strength and performance within the elastic region for polymer samples, particular attention was given to investigating the yield strength value, while the ultimate strength was not reported. Also, the provided strain corresponds to the sample's strain at the yield point.

Based on the obtained results, the yield strength of the HP 552R sample measured 29.2 MPa. Upon the addition of reinforcing particles and fibers, there were noticeable variations in yield strength. With the inclusion of $CaCO_3$ particles, a decline in yield strength was observed. Specifically, the yield strength of the sample containing 30% $CaCo_3$ decreased to 27.5 MPa, representing a 5.8% reduction compared to the HP 552R sample. Similarly, increasing

FIGURE 6 | (a) The furnace, (b) the crucible, and (c) the ash residue from the samples.

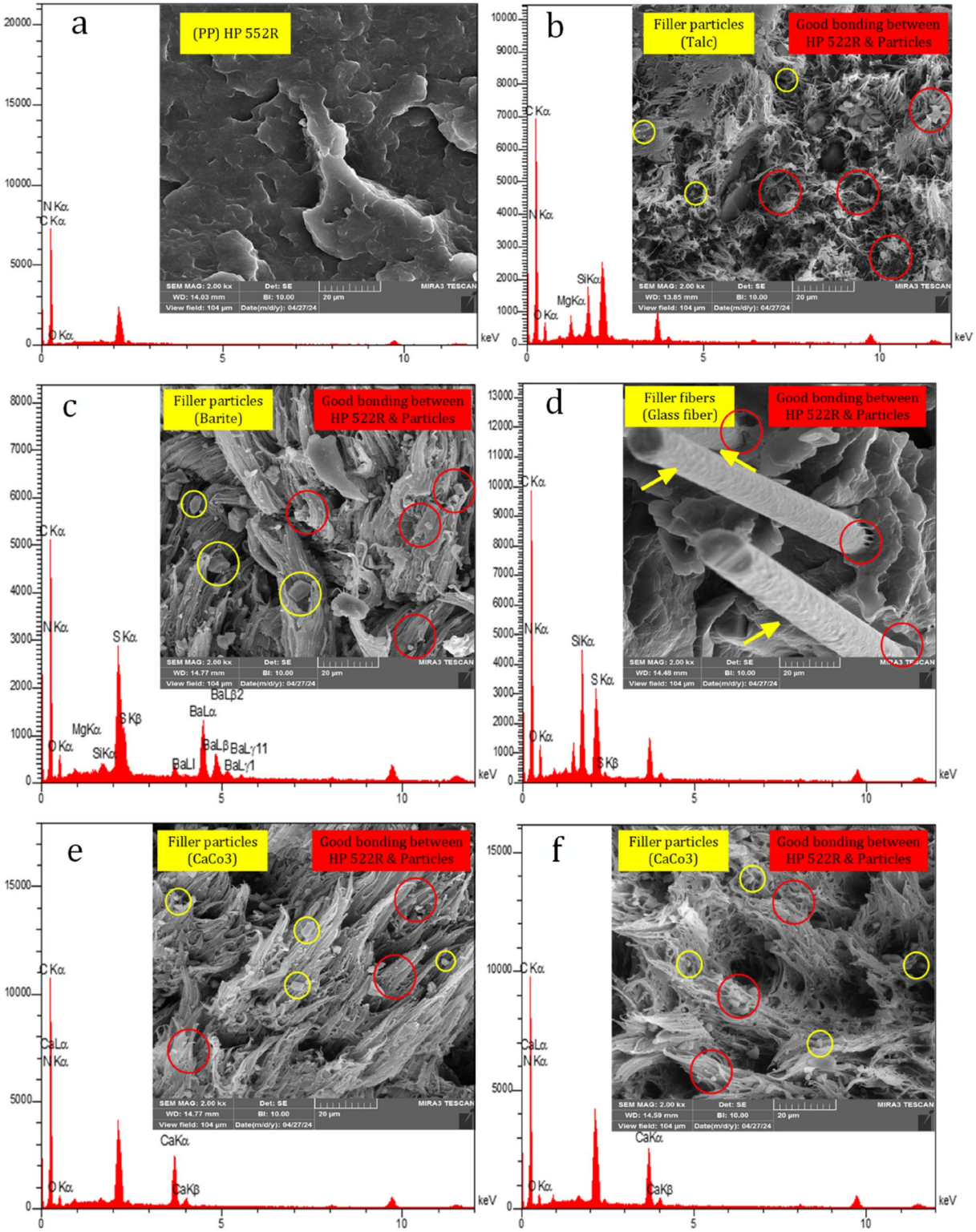

FIGURE 7 | The EDS graph and SEM image with 20 μm magnification of (a) (PP) HP 552R, (b) 20% talc, (c) 20% barite, (d) GF30% [L/D = 300], (e) 30% $CaCo_3$, and (f) 20% $CaCo_3$.

the percentage of $CaCO_3$ particles from 20% to 25% resulted in marginal changes, with yield strengths of 27.8 and 27.6 MPa, respectively. A similar decreasing trend in yield strength was noted in the 20% barite sample, where the yield strength decreased to 24.4 MPa, marking a 16.4% reduction compared to the HP 552R sample. This decline in yield strength can be attributed to the addition of $CaCO_3$ and barite particles, which each possess lower yield strengths, consequently leading to a decrease in the overall strength of the produced samples [26]. Also, the declining trend in yield strength with an increasing percentage of $CaCo_3$ particles is due to the "clumping" (i.e., the agglomeration of particles within the matrix). However, upon the addition of talc particles as well as GFs to the PP matrix, there was an increase in yield strength. For instance, in two different samples containing 20% talc and GF30%

[L/D = 250], the yield strength increased by 10% and more than doubled compared to the HP 552R sample, respectively. This is due to the effective transfer of force to the reinforcements during loading. On the other hand, barite and $CaCo_3$ particles possess a spherical shape, whereas talc particles exhibit an approximate cuboid morphology. In tensile testing, talc particles demonstrate superior adhesion with the polymer matrix, resulting in an increased composite strength. However, the weaker adhesion observed in $CaCo_3$ and barite particles renders them susceptible to separation upon the application of tensile forces. Thus, from a certain point, such separation can occur, leading to the formation of voids that serve as nucleation sites for crack propagation. This phenomenon may consequently result in a reduction in overall composite strength.

TABLE 2 | The tensile test results.

Samples	Young's modulus [MPa]	Yield stress [MPa]	Strain [%]
(PP) HP 552R	1472	29.2	10.4
20% $CaCo_3$	1297	27.8	4.6
25% $CaCo_3$	1289	27.6	4.3
30% $CaCo_3$	1268	27.5	4.1
20% talc	1572	32.4	6.7
20% barite	1429	24.4	4.7
GF30% [L/D = 250]	6687	87.1	5.2
GF30% [L/D = 300]	6871	91.9	5.4
GF30% [L/D = 350]	7629	98.6	5.5

In GF-reinforced composites, an increase in the L/D ratio of the reinforcing GFs leads to a proportional increase in yield strength. In fact, the advantageous aspect lies in the enhanced contact surface area between the fibers and the matrix compared to the particle reinforcements. This augmented interface facilitates superior load transfer efficiency from the matrix to the reinforcement upon application of mechanical forces [20]. A crucial determinant of this interaction is the aspect ratio of the fibers, defined as the ratio of fiber length to diameter. A higher ratio corresponds to a greater surface area-to-volume ratio of the fibers, consequently leading to an increased wettability of the fibers. This phenomenon signifies that a larger portion of fiber surface area becomes engaged with the matrix, thereby contributing to the enhancement of composite strength. The stress–strain diagrams of several samples can be observed in Figure 8.

A similar trend is evident regarding the strain at the yield point and the modulus of elasticity, with the only deviation observed in the strain of GF-reinforced samples: Contrary to the increase in yield strength, the strain at the yield point has decreased. The HP 552R sample exhibited the highest strain equal to 10.4%, while the lowest was recorded for the 30% $CaCo_3$ sample at 4.1%. Among the reinforced samples, the 20% talc sample displayed the highest strain of 6.7%, representing a 42% increase compared to the strain of the 20% barite sample. Generally, the presence of reinforcement particles/fibers serves to constrain the mobility of polymer chains, thereby reducing the extent of strain experienced within the composite material. Furthermore, the GF30% sample [L/D = 350] exhibited the highest elastic modulus of 7629 MPa, representing a more than fivefold increase over the elastic modulus of the HP 552R sample. Figure 9 depicts a visual representation of some sample's failure at the conclusion of the tensile test.

To gain insights into the fracture behavior and characteristics of the samples, SEM imaging was utilized to analyze the fracture

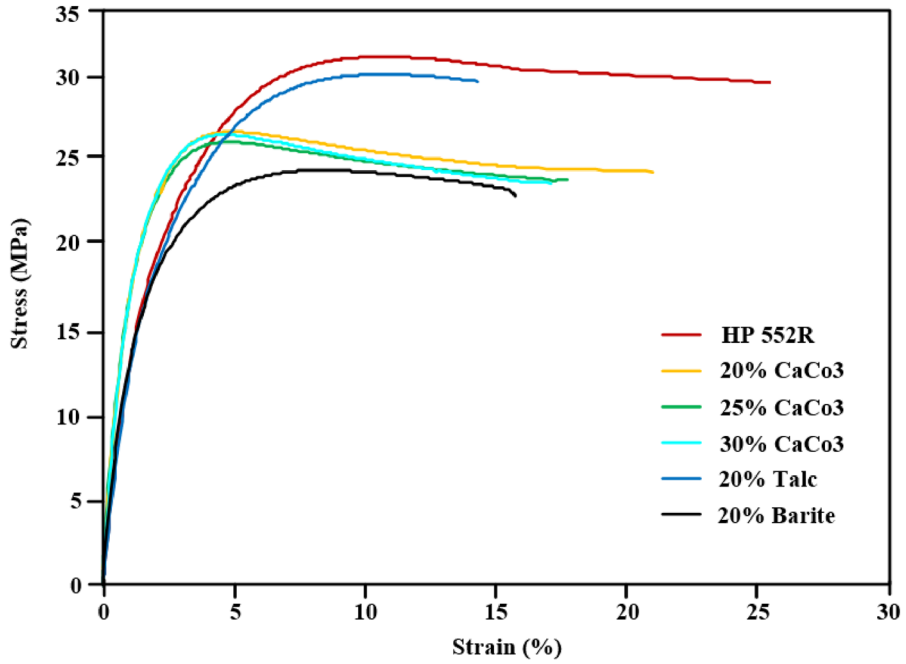

FIGURE 8 | The stress–strain curves of the produced samples.

cross-section of specific samples at two magnifications, 2mm and 100μm, as illustrated in Figure 10. Examination of the fracture surface of the HP 552R sample (PP) indicates a more ductile fracture compared to others, displaying a large plastic deformation, consistent with the observed strain in the tensile test results (Figure 10a). The addition of talc to the matrix reduces strain, as evidenced by less plastic deformation on the fracture surface and a tendency toward embrittlement. The ductile fracture has a significant amount of plastic deformation, and the surface exhibits a rough, fibrous appearance, but the brittle fracture has a little or no plastic deformation prior to fracture, and the surface is typically smooth and flat (Figure 10b). Further reduction in strain is noted with the inclusion of GF30% and barite, leading to a transition from a ductile to a brittle fracture. As shown in Figure 10c, the GFs in the PP matrix is stretched perpendicular to the fracture surface. This indicates the higher strength of the samples containing GFs, which is due to the high contact surface and good bonding of the GFs with the matrix. This becomes more evident with increasing

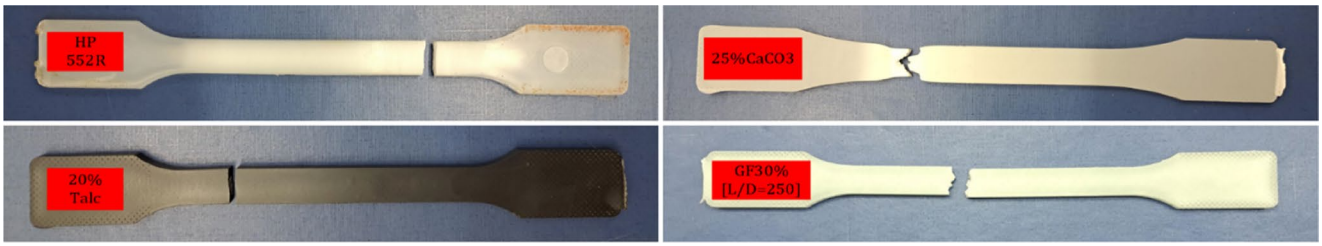

FIGURE 9 | Failure of the sample at the conclusion of the tensile test.

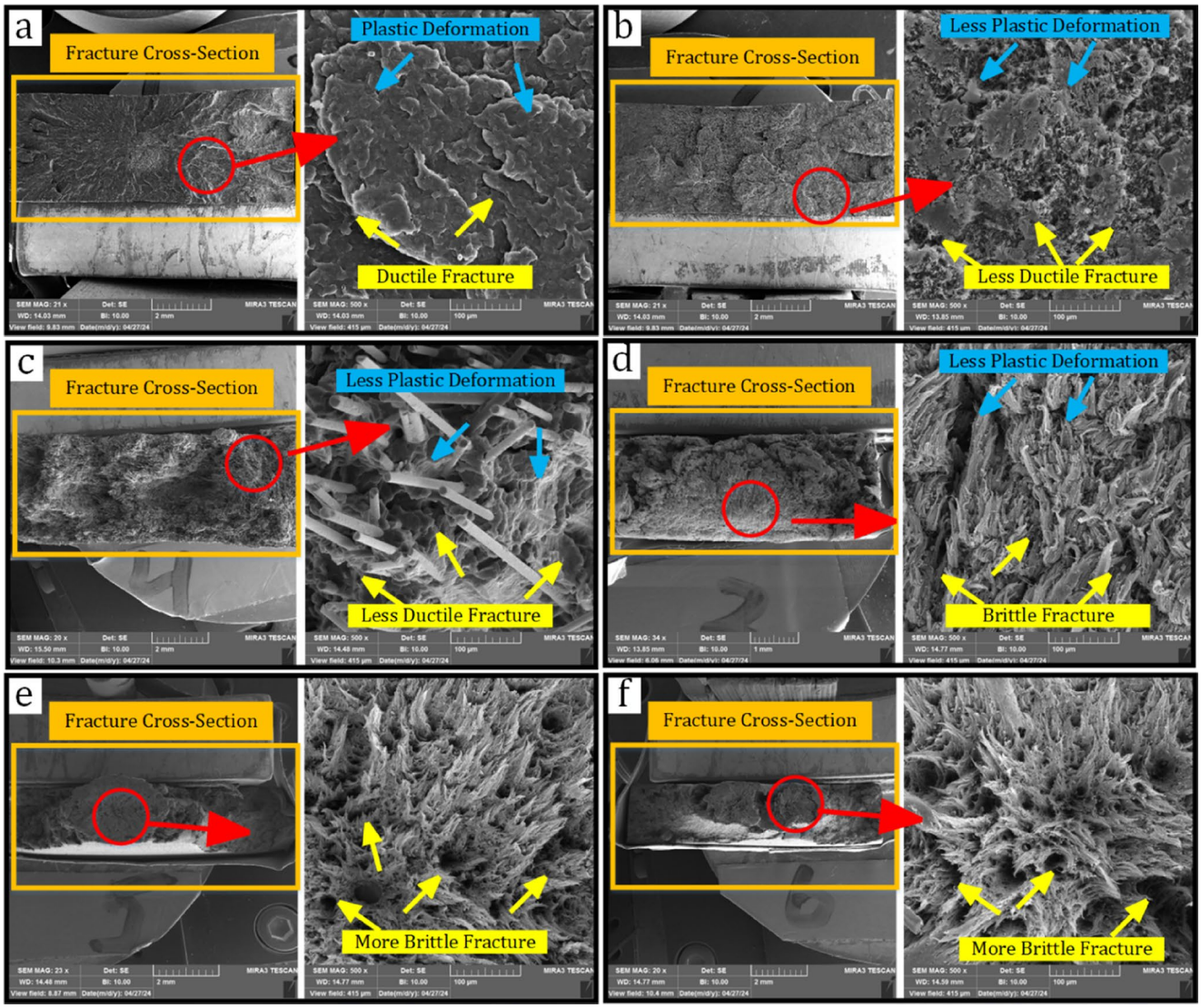

FIGURE 10 | The SEM image of fracture cross-section (a) (PP) HP 552R, (b) 20% Talc, (c) GF30% [L/D = 300], (d) 20% Barite, (e) 30% $CaCo_3$, and (f) 20% $CaCo_3$.

GF length, which is consistent with the values in Table 2. Samples reinforced with $CaCo_3$ exhibit the lowest strain, suggesting a totally brittle failure based on the tensile test results. SEM images of the fracture surface of $CaCo_3$-reinforced samples reveal a porous-type surface. According to Figure 10e,f, the addition of $CaCo_3$ to PP changes the behavior and fracture of the matrix from soft to brittle, and as a result, the strength of the composite material is lower than that of pure PP.

3.3 | Charpy Notched Test

The Charpy impact test was conducted on the produced samples to evaluate their fracure toughness and impact behavior. This test was performed three times for each sample, and the average results are presented in Table 3. It is noteworthy that crucial parameters in the impact test encompass the pendulum speed-at-impact and the amount of absorbed energy, all conducted in accordance with the ISO 179-1 standard.

The energy absorption for the HP 552 sample measured 3.1 kJ/m^2. Upon the addition of talc, the energy absorption decreased by 19% to 2.5 kJ/m^2. However, with the incorporation of other reinforcements, the energy absorption increased. Spherical filler particles (i.e., barite and $CaCo_3$) exhibit an additional enhancement in impact strength within the composite material. Conversely, cubic particles (i.e., talc), possess sharp corners within their geometry, thus serving as stress concentration centers within the matrix. Therefore, these sharp corners facilitate the initiation and propagation of cracks, thereby potentially compromising the material's impact strength. The highest energy absorption was observed for the 30% GF sample [L/D = 350], reaching 14.1 kJ/m^2. This represents a more than 4.5-fold increase compared to the HP 552 sample. The presence of GFs in the matrix plays a pivotal role, as they absorb the incoming force and energy, resulting in enhanced energy absorption. Accordingly, reducing the L/D ratio to 300 and 250 resulted in energy absorption values of 12.9 and 11.2 kJ/m^2, respectively. The addition of $CaCo_3$ to PP did not significantly alter the amount of energy absorption (specifically for 20% and 25% $CaCo_3$ samples). For instance, the energy absorption in the 20% $CaCo_3$ sample increased by 6% compared to the HP 552 sample. Increasing the $CaCo_3$ content to 30% resulted in a 14% increase in energy absorption compared to the 25% $CaCo_3$ sample, reaching 3.9 kJ/m^2. The energy absorption in the 20% barite sample measured 5.1 kJ/m^2, indicating proper dispersion and bonding between the barite particles and the polymer matrix. The image of two samples following the impact test is depicted in Figure 11.

TABLE 3 | The charpy impact test results.

Samples	Enegy absorbtion [kJ/m^2]
(PP) HP 552R	3.1
20% $CaCo_3$	3.3
25% $CaCo_3$	3.4
30% $CaCo_3$	3.9
20% Talc	2.5
20% barite	5.1
30% GF [L/D = 250]	11.2
30% GF [L/D = 300]	12.9
30% GF [L/D = 350]	14.1

3.4 | HDT Test

The HDT test was conducted on all produced samples until their bending deflection reached 0.34 mm. In Figure 12, as an instance, the bending of the sample of 30% GF [L/D = 300] is shown. Additionally, the HDT test results are provided in Table 4.

The lowest temperature required to achieve the desired deflection for the sample HP 552R was 49.8°C, indicating the high sensitivity of raw PP material to heat; with temperatures below 50°C, a deflection of 0.34 mm was attained. However, with the addition of reinforcing particles and fibers, the deflection temperature of the polymer composite samples increased. Among the reinforced samples, the lowest HDT temperature was observed for the 20% barite sample, reaching 57.4°C. Furthermore, adding 25% $CaCo_3$ increased the deflection temperature to 70.1°C, representing a 40% increase compared to the PP sample. This is due to the presence of $CaCo_3$ particles, which are well dispersed and bonded throughout the matrix, thereby increasing the bending strength of the sample and necessitating a higher temperature to reach the standard deflection. However, a significant enhancement in the HDT of PP matrix composite occurs with the addition of GFs. The HDT of the 30% GF [L/D = 350] sample reached 151.7°C, representing a remarkable threefold increase compared to the HP 552R sample. The GFs, arranged in a web-like structure within the matrix and their strong bond with it, contribute to increased bending strength in the samples. In general, the presence of reinforcement materials, typically characterized

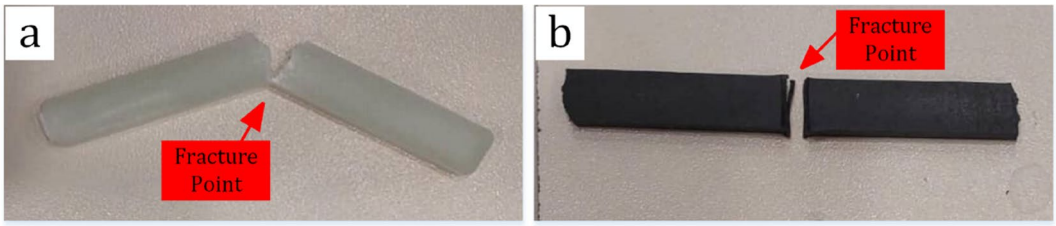

FIGURE 11 | (a) The HP 552 sample and (b) 20% talc after the charpy test.

by higher hardness and superior thermal properties compared to the polymer matrix, contributes to an increase in the HDT of the composite material [31]. This elevation in HDT serves as an indicator of the material's enhanced thermal resistance, highlighting the beneficial effects of reinforcement on thermal performance.

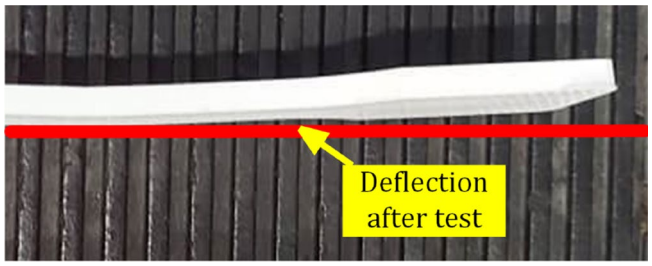

FIGURE 12 | The 30% GF [L/D = 300] sample after the HDT test.

TABLE 4 | The HDT test results.

Samples	Heat deflection temperature [°c]
(PP) HP 552R	49.8
20% $CaCo_3$	67.4
25% $CaCo_3$	70.1
30% $CaCo_3$	71.4
20% Talc	78.4
20% barite	57.4
30% GF [L/D = 250]	139.4
30% GF [L/D = 300]	145.2
30% GF [L/D = 350]	151.7

3.5 | Shrinkage Test

Given that shrinkage is a critical parameter influencing polymer samples and should be considered during part design, a shrinkage test was conducted on the composite samples. The results are illustrated in Figure 13.

Nonuniform shrinkage in polymer parts can induce tension, resulting in longitudinal and transverse cracks. Crystalline polymer samples typically exhibit higher shrinkage compared to semicrystalline and amorphous polymers, as semicrystalline polymers partially restore their macroscopic structure during cooling. Then, the crystallization rate inversely correlates with shrinkage; lower crystallinity leads to reduced shrinkage. For instance, the crystalline HP 552R sample exhibited a shrinkage of 1.91%, which decreased to 1.72% with the addition of 20% $CaCo_3$ to the matrix. Further addition of $CaCO_3$ had minimal effect on shrinkage, with samples containing 25% and 30% $CaCo_3$ exhibiting a shrinkage of 1.6%. The 20% barite sample exhibited a shrinkage of 1.72%, whereas the addition of talc led to a decrease in shrinkage to 1.42% in the 20% talc sample. This difference is due to the layered structure and higher softness and slipperiness of talc particles compared to barite, resulting in reduced viscosity and friction during particle movement. Incorporating GFs into the PP significantly reduces shrinkage. For instance, the 30% GF [L/D = 350] sample displays a mere 0.26% shrinkage, marking over a sevenfold decrease compared to the HP 552R sample. Furthermore, decreasing the L/D ratio of GFs slightly increased shrinkage, reaching 0.34% in the 30% GF [L/D = 300] sample. In the context of shrinkage, the incorporation of fibers and particles serves to mitigate the shrinkage. This reduction is attributed to the particles' ability to restrict the movement of the polymer matrix, particularly from the contact side, thus constraining shrinkage to occur predominantly in the free direction. Notably, this effect is particularly pronounced with GFs, owing to their extensive contact surface area compared to other particles, which effectively curtails the mobility of the polymer matrix.

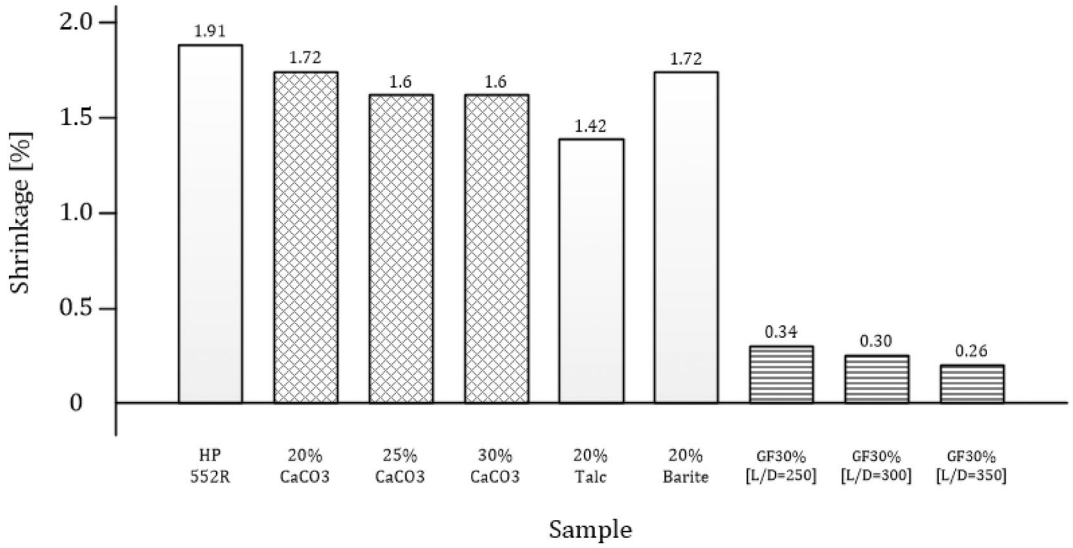

FIGURE 13 | The shrinkage test results.

3.6 | MFI Test

The ease of melt flow was evaluated through the MFI test conducted on the samples. An image displaying the remaining samples extracted from the orifice is presented in Figure 14. Furthermore, the results of the MFI test are illustrated in Figure 15.

Temperature and time play crucial roles in the MFI test, where the ease of melt flow for the HP 552R sample is measured at 25.4 g/10 min. Incorporating a small amount of calcium carbonate into the matrix marginally reduces the ease of melt flow, as evidenced by the 20% $CaCo_3$ sample registering a rate of 23.2 g/10 min, approximately 9% lower than that of the HP 552R sample. In general, the incorporation of calcium carbonate tends to enhance the ease of melt flow by augmenting the molecular weight of the resulting sample, consequently leading to a reduction in viscosity. Interestingly, the ease of melt flow remains consistent for the samples with 25% and 30% $CaCo_3$, both recording rates of 26.1 and 25.9 g/10 min, respectively. Similarly, the presence of barite particles increases the ease of melt flow by 4.7%, resulting in a value of 26.6 g/10 min for the 20% barite sample. Conversely, the incorporation of GFs causes a substantial reduction in the ease of melt flow, with the 30% GF [L/D = 350] sample exhibiting the lowest melt flow rate at 5.2 g/10 min. In the context of MFI, the inclusion of GFs serves a dual role: firstly, by impeding the mobility of polymer chains, and secondly, by hindering the unrestricted flow of the polymer in its molten state. Indeed, the incorporation of GFs within the polymer melt resembles an obstructive barrier, akin to an impediment encountered at the exit nozzle of a processing device. This phenomenon leads to a reduction in the MFI index and an increase in viscosity. Furthermore, reducing the L/D ratio of GFs leads to a slight increase in the MFI value, with the 30% GF [L/D = 250] sample recording a value of 6.4 g/10 min.

FIGURE 14 | Remaining samples of 20% talc extracted from the orifice after MFI test.

3.7 | Ash Content Test

The ash content test was conducted to determine the residue ash left in the samples, with the results illustrated in Figure 16. As elaborated in Section 2, the initial samples (i.e., PP HP 552R) were devoid of any additives, yielding an expected ash content of zero. Thus, upon introducing reinforcement additives to produce composite samples, the ash content proportionally increased. For instance, the ash content for the 25% and 30% $CaCo_3$ samples amounted to 24.2% and 31.4%, respectively. Similarly, the inclusion of talc and barite reinforcing particles resulted in elevated ash content, with marginal disparity observed between the 20% talc and 20% barite samples, yielding 19.8% and 20.5%, respectively. This trend persisted in samples reinforced with GFs, where comparable ash content was recorded across varying L/D ratios, with values of 35.2% for the 30% GF sample [L/D = 250] and 35.3% for the 30% GF sample [L/D = 350].

4 | Conclusion

This study investigated the influence of various reinforcing materials, including $CaCo_3$, talc, barite, and GF on the mechanical and thermal properties of HP 552R PP matrix composites.

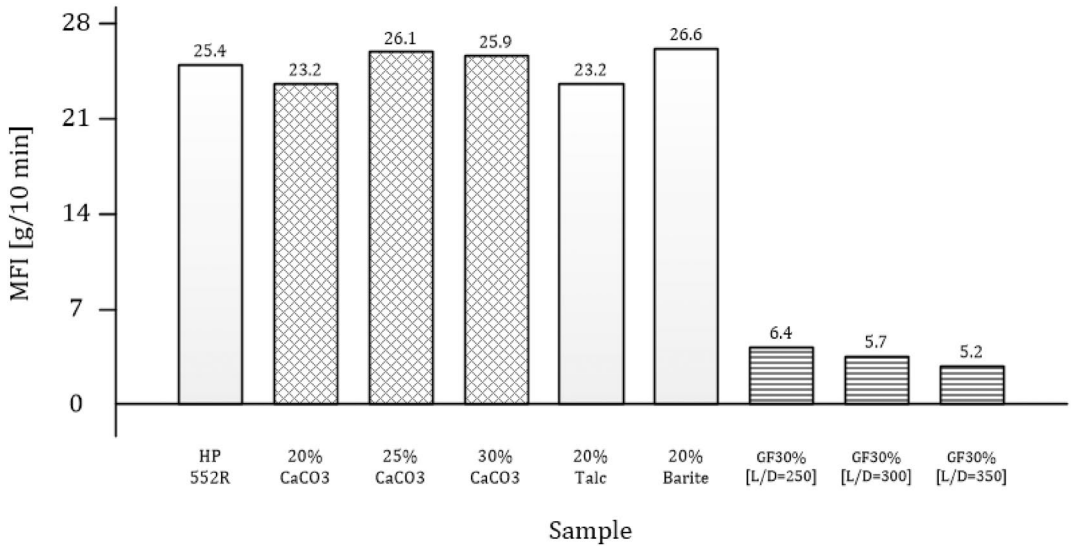

FIGURE 15 | The MFI test results.

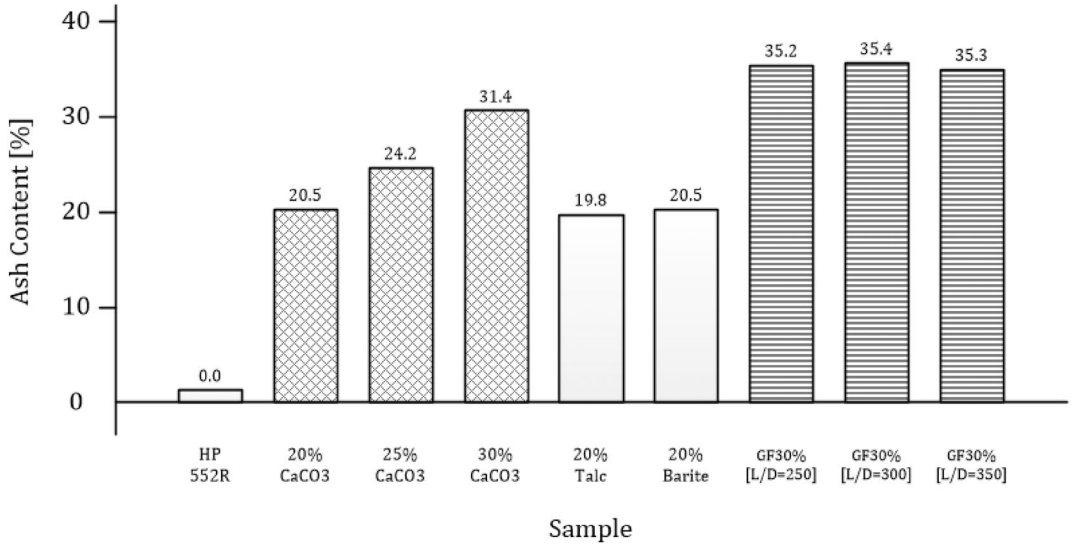

FIGURE 16 | The ash content test results.

The results demonstrated that the incorporation of GFs significantly enhanced the mechanical properties, while particulate fillers improved thermal properties. Some of the obtained results are listed:

1. Generally, the addition of reinforcing particles led to a reduction in the yield strain of the samples. For instance, the strain values ranged from 10.4% for the HP 552R sample (with no added reinforcing material) to 4.1% for the 30% $CaCo_3$ sample. Conversely, the yield strength exhibited notable variations across the samples, with the highest recorded at 98.6 MPa for the 30% GF sample [L/D = 350], while the lowest was observed for the 20% barite sample, registering at 24.4 MPa.
2. Charpy impact test findings revealed that the energy absorption of the HP 552 sample measured at 3.1 kJ/m^2, while the addition of 20% talc resulted in a reduction to 2.5 kJ/m^2. Interestingly, the inclusion of $CaCo_3$ did not significantly impact energy absorption, but the 30% GF sample [L/D = 350] exhibited the highest energy absorption of 14.1 kJ/m^2.
3. In the HDT test, the temperature required to induce a 0.34 mm bending deflection in the HP 552R sample was 49.8°C. However, with the incorporation of reinforcing particles and fibers, the HDT notably increased. For instance, the maximum temperature recorded was 151.7°C for the 30% GF [L/D = 350] sample.
4. Ideally, polymer materials should exhibit low shrinkage, and the incorporation of reinforcing particles and GFs has effectively reduced shrinkage. Notably, while the HP 552R sample displayed a shrinkage rate of 19.1%, this figure significantly decreased to 1.42% and 0.26% for the 20% talc and 30% GF [L/D = 350] samples, respectively.
5. The ease of melt flow was assessed through the MFI test for the composite samples. While the MFI for the HP 552R sample stood at 25.4 g/10 min, the addition of $CaCo_3$, talc, and barite particles did not significantly alter the MFI. Conversely, incorporating GFs into the matrix led to a reduction in MFI, with the 30% GF [L/D = 350] sample recording a value of 5.2 g/10 min.
6. The introduction of reinforcing particles and GFs resulted in increased ash content. Notably, the 30% GF [L/D = 300] sample exhibited the highest ash content at 35.6%.

These findings provide valuable insights for the design and optimization of PP-based composites for a wide range of applications. Future research could focus on optimizing the fiber orientation and distribution, exploring hybrid reinforcement systems, and investigating the effects of surface modification on the interfacial bonding between the reinforcement and the matrix.

Ethics Statement

The authors have nothing to report.

Conflicts of Interest

The authors declare no conflicts of interest.

Data Availability Statement

The data that support the findings of this study are available on request from the corresponding author. The data are not publicly available due to privacy or ethical restrictions.

References

1. K. Rahmani, A. Nouri, H. Bakhtiari, et al., "Mechanical and Corrosion Properties of Mg–MgO and Mg–Al2O3 Composites Fabricated by Equal Channel Angular Extrusion Method," *Smart Materials in Manufacturing* 1 (2023): 100010.

2. Z. Yin, D. Wei, Q. Lin, et al., "Synergistic Toughening Effects of Elastomer Toughener and Nucleating Agent on Mechanical Properties and Crystallization Behaviors of Polypropylene," *Polymers for Advanced Technologies* 35, no. 9 (2024): e6578.

3. S. J. Hashemi, A. Sadooghi, K. Rahmani, and S. Nokhbehroosta, "Experimental Determining the Mechanical and Stiffness Properties of

Natural Rubber FRT Triangle Elastic Joint Composite Reinforcement by Glass Fibers and Micro/Nano Particles," *Polymer Testing* 85 (2020): 106461.

4. J.-L. Zhang and X.-H. Li, "Preparation and Characterization of Nano-Filled Polypropylene Dielectric Films," *Polymers for Advanced Technologies* 35, no. 8 (2024): e6534.

5. K. Baek, H. Kim, H. Shin, H. Park, and M. Cho, "Multiscale Study to Investigate Nanoparticle Agglomeration Effect on Electrical Conductivity of Nano-SiC Reinforced Polypropylene Matrix Composites," *Mechanics of Advanced Materials and Structures* 30, no. 12 (2023): 2442–2452.

6. V. Zal and M. Yasaee, "A New Light Transmission Method to Evaluate the Through Thickness Fibre Alignment in Transparent Resin," *Composites Part A: Applied Science and Manufacturing* 159 (2022): 107000.

7. V. Zal, H. Moslemi Naeini, A. R. Bahramian, A. H. Behravesh, and B. Abbaszadeh, "Investigation and Analysis of Glass Fabric/PVC Composite Laminates Processing Parameters," *Science and Engineering of Composite Materials* 25, no. 3 (2018): 529–540.

8. S. Begum, S. Fawzia, and M. S. J. Hashmi, "Polymer Matrix Composite With Natural and Synthetic Fibres," *Advances in Materials and Processing Technologies* 6, no. 3 (2020): 547–564.

9. M. Małek, W. Łasica, M. Kadela, J. Kluczyński, and D. Dudek, "Physical and Mechanical Properties of Polypropylene Fibre-Reinforced Cement–Glass Composite," *Materials* 14, no. 3 (2021): 637.

10. A. Ari, A. Bayram, M. Karahan, and S. Karagöz, "Comparison of the Mechanical Properties of Chopped Glass, Carbon, and Aramid Fiber Reinforced Polypropylene," *Polymers and Polymer Composites* 30 (2022): 09673911221098570.

11. J. Guo, M. Cao, W. Ren, H. Wang, and Y. Yu, "Mechanical, Dynamic Mechanical and Thermal Properties of TiO2 Nanoparticles Treatment Bamboo Fiber-Reinforced Polypropylene Composites," *Journal of Materials Science* 56, no. 22 (2021): 12643–12659.

12. V. Goud, R. Alagirusamy, A. das, and D. Kalyanasundaram, "Influence of Various Forms of Polypropylene Matrix (Fiber, Powder and Film States) on the Flexural Strength of Carbon-Polypropylene Composites," *Composites Part B: Engineering* 166 (2019): 56–64.

13. K. Hariprasad, K. Ravichandran, V. Jayaseelan, and T. Muthuramalingam, "Acoustic and Mechanical Characterisation of Polypropylene Composites Reinforced by Natural Fibres for Automotive Applications," *Journal of Materials Research and Technology* 9, no. 6 (2020): 14029–14035.

14. N. Song, D. Cao, X. Luo, Q. Wang, P. Ding, and L. Shi, "Highly Thermally Conductive Polypropylene/Graphene Composites for Thermal Management," *Composites Part A: Applied Science and Manufacturing* 135 (2020): 105912.

15. I. O. Oladele, I. O. Ibrahim, A. D. Akinwekomi, and S. I. Talabi, "Effect of Mercerization on the Mechanical and Thermal Response of Hybrid Bagasse Fiber/$CaCO_3$ Reinforced Polypropylene Composites," *Polymer Testing* 76 (2019): 192–198.

16. J. A. Hernández-Jiménez, R. M. Jiménez-Amezcua, M. G. Lomelí-Ramírez, J. A. Silva-Guzmán, J. G. Torres-Rendón, and S. García-Enriquez, "Utilization of Wood Flour From White Oak Branches as Reinforcement in a Polypropylene Matrix: Physical and Mechanical Characterization," *Journal of Composites Science* 6, no. 7 (2022): 184.

17. J. Korol, A. Hejna, D. Burchart-Korol, and J. Wachowicz, "Comparative Analysis of Carbon, Ecological, and Water Footprints of Polypropylene-Based Composites Filled With Cotton, Jute and Kenaf Fibers," *Materials* 13, no. 16 (2020): 3541.

18. K.-W. Kim, W. Han, and B.-J. Kim, "Effects of Mixing Ratio of Hybrid Carbonaceous Fillers on Thermal Conductivity and Mechanical Properties of Polypropylene Matrix Composites," *Polymers* 14, no. 10 (2022): 1935.

19. G. Rajkumar, G. K. Sathishkumar, K. Srinivasan, et al., "Structural and Mechanical Properties of Lignite Fly Ash and Flax-Added Polypropylene Polymer Matrix Composite," *Journal of Natural Fibers* 19, no. 13 (2022): 6534–6552.

20. P. B. Patel, A. K. Chandra, G. K. Pandey, et al., "Influence on the Mechanical Properties of Polymetric Matrix Composites With Different Types of Reinforcing Loads," *Materials Today Proceedings* (2023), https://doi.org/10.1016/j.matpr.2023.08.072.

21. S. Brahma, S. M. Raafi, S. N. Arju, and J. u. Rehman, "Dyeability and Mechanical Properties of Banana Fiber Reinforced Polypropylene Composite," *SPE Polymers* 5 (2024): 353–365.

22. R. Meena, A. W. Hashmi, S. Ahmad, et al., "Influence of Fly Ash on Thermo-Mechanical and Mechanical Behavior of Injection Molded Polypropylene Matrix Composites," *Chemosphere* 343 (2023): 140225.

23. L. Xiao, F. Liang, and Z. Zhou, "Effects of Compound Compatibilizer and CaTiO3 Filler on the Properties of Polypropylene/Polyphenylene Ether/Glass Fiber Composites," *Polymer Composites* 45, no. 12 (2024): 11093–11103.

24. M. R. Lombardo, B. Callegari, E. B. Ferreira, et al., "Effect of Borosilicate Residue as Flame Retardant and Reinforcement Filler in Polypropylene/Natural Fiber Composites," *Journal of Applied Polymer Science* 141 (2024): e56166.

25. K. V. Balaji, K. Shirvanimoghaddam, R. Yadav, R. Mahmoodi, V. Unnikrishnan, and M. Naebe, "The Synergy of the Matrix Modification and Fiber Geometry to Enhance the Thermo-Mechanical Properties of Basalt Fiber-Polypropylene Composites for Automotive Applications," *Journal of Applied Polymer Science* 141 (2024): e55682.

26. K. Yang, Q. Yang, G. Li, Y. Sun, and D. Feng, "Morphology and Mechanical Properties of Polypropylene/Calcium Carbonate Nanocomposites," *Materials Letters* 60, no. 6 (2006): 805–809.

27. K. Palanikumar, R. AshokGandhi, B. K. Raghunath, and V. Jayaseelan, "Role of Calcium Carbonate ($CaCO_3$) in Improving Wear Resistance of Polypropylene (PP) Components Used in Automobiles," *Materials Today Proceedings* 16 (2019): 1363–1371.

28. Y. Zhou, V. Rangari, H. Mahfuz, S. Jeelani, and P. K. Mallick, "Experimental Study on Thermal and Mechanical Behavior of Polypropylene, Talc/Polypropylene and Polypropylene/Clay Nanocomposites," *Materials Science and Engineering A* 402, no. 1–2 (2005): 109–117.

29. L. Lapcik, P. Jindrova, B. Lapcikova, et al., "Effect of the Talc Filler Content on the Mechanical Properties of Polypropylene Composites," *Journal of Applied Polymer Science* 110, no. 5 (2008): 2742–2747.

30. S.-Y. Fu, B. Lauke, E. Mäder, C. Y. Yue, and X. Hu, "Tensile Properties of Short-Glass-Fiber-and Short-Carbon-Fiber-Reinforced Polypropylene Composites," *Composites Part A: Applied Science and Manufacturing* 31, no. 10 (2000): 1117–1125.

31. A. Sadooghi, K. Rahmani, and S. J. Hashemi, "Effects of Nano and Micro Size of MgO on Mechanical Properties, Wear, and Corrosion of Magnesium Matrix Composite," *Strength of Materials* 53, no. 6 (2021): 983–997.